DOI: 10.3901/CJME.2010.0*.***, available online at www.cjmenet.com; www.cjmenet.com.cn

Adsorption Performance of Sliding Wall-Climbing Robot

LI Jun[1], GAO Xueshan[1,*], FAN Ningjun[1], LI Kejie[1], JIANG Zhihong[1] and JIANG Zhijian[2]

1 *School of Mechatronical Engineering, Beijing Institute of Technology, Beijing 100081, China*
2 *School of Electric and Information Engineering, Beijing University of Civil Engineering and Architecture, Beijing 100044, China*

Received April 8, 2010; revised October 28, 2010; accepted November **, 2010; published electronically November **, 2010

Abstract: Sliding wall-climbing robot (SWCR) is applied worldwide for its continuous motion, however, considerable air leakage causes two problems: great power consumption and big noise, and they constraint the robot's comprehensive performance. So far, effective theoretical model is still lacked to solve the problems. The concept of SWCR's adsorption performance is presented, and the techniques of improving utilization rate of given adsorption force and utilization rate of power are studied respectively to improve SWCR's adsorption performance. The effect of locomotion mechanism selection and seal's pressure allocation upon utilization rate of given adsorption force is discussed, and the theoretical way for relevant parameters optimization are provided. The directions for improving utilization rate of power are pointed out based on the detail analysis results of suction system's thermodynamics and hydrodynamics. On this condition, a design method for SWCR-specific impeller is presented, which shows how the impeller's key parameters impact its aerodynamic performance with the aid of computational fluid dynamics (CFD) simulations. The robot prototype, BIT Climber, is developed, and its functions such as mobility, adaptability on wall surface, payload, obstacle ability and wall surface inspection are tested. Through the experiments for the adhesion performance of the robot adsorption system on the normal wall surface, at the impeller's rated rotating speed, the total adsorption force can reach 237.2 N, the average effective negative pressure is 3.02 KPa and the design error is 3.8% only, which indicates a high efficiency. Furthermore, it is found that the robot suction system's static pressure efficiency reaches 84% and utilization rate of adsorption force 81% by the experiment. This thermodynamics model and SWCR-specific impeller design method can effectively improve SWCR's adsorption performance and expand this robot applicability on the various walls. A sliding wall-climbing robot with high adhesion efficiency is developed, and this robot has the features of light body in weight, small size in structure and good capability in payload.

Key words: wall-climbing robot, adsorption performance, centrifugal impeller, CFD simulation

1 Introduction

There are a variety of tasks that need to be addressed on the inner/outer wall surfaces of high-rise buildings, such as non-destructive testing of chemical storage facilities, cleaning and maintenance of structures in city, material or information transmission in high-altitude rescue, urban anti-terrorism missions. For the purpose of ensuring the operation safety in extreme environments or improve benefit-cost ratio, wall-climbing robot (WCR) is used to accomplish these tasks. According to adsorption method, WCRs can be roughly divided into magnetic adsorption[1–4], bionic adsorption[5–8] and vacuum adsorption. Vacuum adsorption is further divided into high-vacuum[9–17] and low-vacuum[18–25] suction type. Compared with the former, low-vacuum robot does not request strict seal between sucker and wall, so dynamic seal is enough to meet the need, which means that continuous and relative movement exists between robot body and wall, and low-vacuum robot may also be known as the sliding wall-climbing robot (SWCR).

Though the vacuum level in sucker of SWCR is relatively low, it often requires a larger airflow to serve in suction system due to the dynamic seal which results in noticeable shortcomings—great power consumption and big noise which seriously restricts the robot's overall performance, so the problem how to improve the adsorption performance becomes a key technique that should be considered. SWCR's adsorption performance contains two aspects:

(1) Suction system's ability to turn power consumed by gas source machinery (usually impeller) into adsorption force, called the utilization rate of power;

(2) Mainbody's ability to turn adsorption force into propulsion, called the utilization rate of adsorption force.

A lot of efforts are made to improve SWCR's adsorption performance. "City Climber" robots [19–20] have experienced the development of type I, II, III. City Climber I uses a soft brush sealing skirt to avoid the problem that robot using pneumatic tyre as seal tends to get stuck when adsorption force is too big, allowing the robot to work in high-suction

* Corresponding author. E-mail: xueshan.gao@bit.edu.cn
This study is supported by Ministry of Housing and Urban-Rural Development of China (Grant No. 2007-k8-6) and National Natural Science of Foundation of China (Grant No. 60975070)

state to increase load capacity. In addition, the robot is equipped with a novel device connecting vacuum chamber with seal—the isolation ring which is made from foam and plays a key role in optimizing the distribution of adsorption reaction force on wheels and seal, improving the utilization rate of adsorption and enhancing the locomotion ability. Three wheels are placed on both sides of City Climber III's body. The middle wheel is independently controlled by motor, while the front and the rear are connected with the middle through a belt, which not only increases the contact friction, but also avoids the wheels' skid. Such mechanism can actually improve the capability of turning adsorption force into static friction (propulsion). Alicia II[23–24] uses a sealing device of "sandwich" structure made from teflon/bristle. From the perspective of adsorption performance, this "maze"-type seal with a high flow resistance is able to maintain vacuum enough in the sucker at a small leakage rate. In addition, Alicia II makes use of special ball bearings to maintain balance with two differential-driving wheels placed on the body's middle line, and this geometric distribution turns adsorption into available friction force to the greatest degree. In 2008, HILLENBRAND, et al[22], developed CROMSCI, 80 cm in diameter and 25 kg in mass, for large-scale concrete construction testing. In order to ensure its reliable adhesion, the vacuum chamber is physically separated into one large cavity and seven small ones, the large cavity joints gas source and seven small cavities which directly contact with the wall. When some of the small cavities fail to keep vacuum enough, the control system will close corresponding channels according to the signals of feedback sensors, thus it will ensure the overall suction reliability. So far, all attempts made in these robots enhance adsorption performance objectively, but theoretical foundation is still lacked to guide practicing.

This paper presents the conception of SWCR's adsorption performance, discussing technical means and theoretical methods to improve its adsorption performance in the two aspects mentioned previously. The paper is arranged as follows: Section 2 discusses how to turn as much as possible adsorption force into driving force. Section 3 builds thermodynamics and hydrodynamics models of centrifugal-impeller based suction system, seeks ways of improving the utilization rate of power. With the aid of computational fluid dynamics (CFD) simulation, section 4 puts forward a design method for SWCR-specific centrifugal impeller, aiming at improving efficiency under a certain flow rate. Section 5 introduces a prototype "BIT Climber" developed by our laboratory and discusses related tests. Finally, experimental results, conclusions and future work are given in section 6.

2 Distribution of Given Adsorption Force

Adsorption force F_a of SWCR refers to the force perpendicular to the wall caused by pressure difference between inside and outside of the chamber. Usually, when robot adheres to the wall, F_a is balanced by three forces together, as shown in Fig. 1:

(1) Supporting force on driven wheels is F_{sd}, which can be turned into static friction force and is the only source of robot's propulsion and load capability, it's a necessary part of adsorption force;

(2) Supporting force on passive wheel is F_{sp},

(3) Supporting force on seal is F_{ss}.

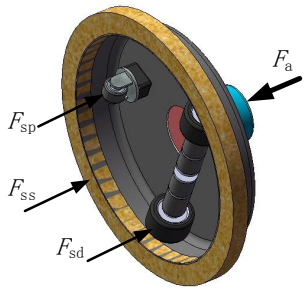

Fig. 1. Equilibrants for adsorption force

Ideally, balance force for F_a contains only F_{sd}, because F_{sp} and F_{ss} can not be transformed into load capacity and mobility, moreover, when the robot moves, F_{ss} will bring additional sliding frictional resistance. From this point of view, the ratio η_a of F_{sd} to F_a should be as large as possible.

However, the existence of the passive wheel not only brings on simplification of the robot's locomotion mechanism and reduces the complexity of control, but also prevents lateral sliding of wheels to ensure control precision[19–20]. And F_{ss} can increase the flow resistance of sealing device, which is favorable to reducing the adsorption power[21, 25].

2.1 Locomotion mechanism

Four kinds of locomotion mechanism are raised as shown in Fig. 2, *a*, *b* have lower utilization rate of adsorption force, but they have the advantages of simple structure and control method.

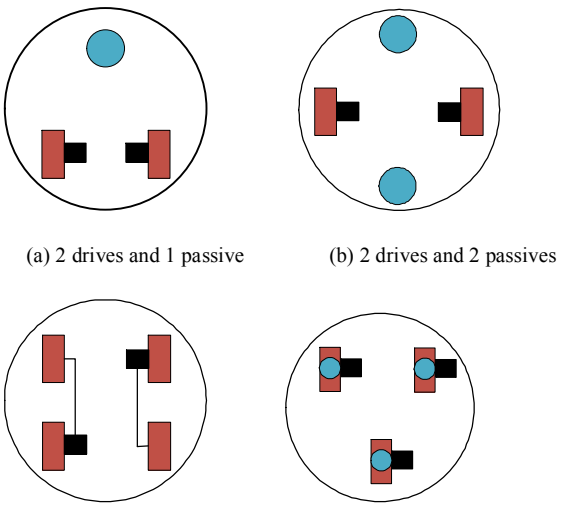

(a) 2 drives and 1 passive (b) 2 drives and 2 passives

(c) 2 drives with belt (d) 3 steering drives

Fig. 2. Diagram of mobile mechanism

If the robot needs an independent implementation of a long time task, the pursuit of low noise and high adsorption performance requirements, *c* or *d* type should be chosen, because they have high utilization rate of adsorption force.

Now we analyse the impact of mechanical parameters on utilization rate of adsorption force when the passive wheel is used. To simplify the problem, in Fig. 3, F_{ss} is neglected. *O* represents center of gravity (CG) of the robot, point *A* is the intersection of driven wheels' axis and mainbody's center line, h_g is the distance from *O* to the wall, b_1 is the distance from *O* to drive wheel's axis, b_2 is the distance from *O* to passive wheel's axis. According to Newtonian mechanics,

$$F_a = 2F_{sd} + F_{sp}, \tag{1}$$

$$F_a b_1 + Gh_g = F_{sp}(b_1 + b_2). \tag{2}$$

From Eqs. (1), (2),

$$F_{sd} = \frac{F_a b_2 - Gh_g}{2(b_1 + b_2)}. \tag{3}$$

According to Eq. (3), we can get the following conclusions: when F_a remains a constant, in order to have a greater driving force, b_2 should be increased and b_1, h_g reduced. Therefore, in locomotion type *b*, b_1 is set to 0, which greatly enhances the utilization rate of adsorption force compared to type *a*.

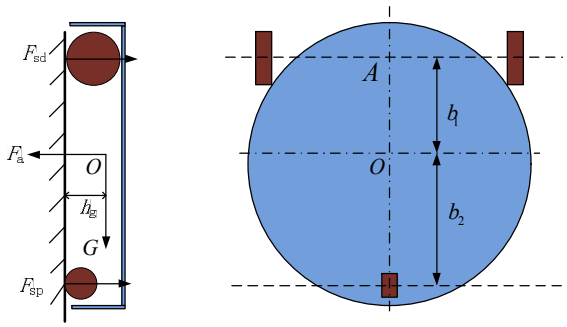

Fig. 3. Statics diagram for SWCR with passive wheel

2.2 Sealing device

After the selection of locomotion mechanism, the issue of seal's pressure allocation needs to be considered, that is, how to set the ratio k_s of F_{ss} to F_a:

$$F_{ss} = k_s F_a, \tag{4}$$

$$F_{sd} = (1 - k_s) F_a. \tag{5}$$

In Fig. 4, assuming the robot's vertical uniform motion upward the wall, from Newton's second law:

$$\mu_d F_{sd} = G + \mu_s F_{ss}, \tag{6}$$

where μ_d is friction coefficient between drive wheel and wall, μ_s is friction coefficient between seal and wall. From Eqs. (4–6),

$$F_a = \frac{G}{\mu_d - (\mu_d + \mu_s)k_s}. \tag{7}$$

Eq. (7) shows that, the smaller k_s gets, the bigger supporting force will be allotted on driven wheels. Moreover, the frictional resistance of sliding seal will get reduced as k_s does, so that the value of F_a that is necessary to make the robot adhere reliably can be made smaller, which is helpful for power saving. However, a too small k_s will cause a sharp reduction in flow resistance, which would substantially increase the suction power and have a pernicious influence on suction system's aerodynamic performance. QIN, et al[25], studied the effect of k_s on suction power of an SWCR robot which uses a pneumatocyst ring as seal, it turns out that, when k_s is within 0.35–0.5, the suction power can be maintained at a relatively low level. The labyrinth-type sealing element could keep k_s at a lower range.

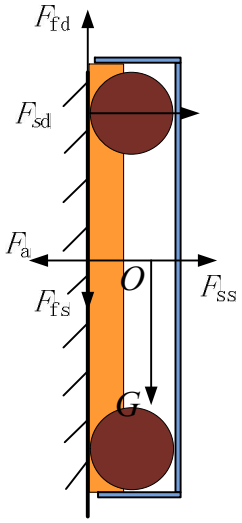

Fig. 4. Force analysis for SWCR with seal on

3 SWCR Suction System Using Centrifugal Impeller

This section will take suction system as research object, in-depth study the formation principle of adsorption force, describe fluid state changes in the suction circuit from the thermodynamical and hydromechanical point of view, present the factors that determine the value of F_a and theoretical method to lower power consumption under the

same F_a.

3.1 Thermodynamical process in the suction circuit

Fig. 5 depicts physical constitution of suction system: sealing, mainbody, and impeller. Under the drive of the centrifugal fan impeller at high rotary speed, external atmospheric air (state A) flows into the chamber through the sealing component (state B), airflow's static pressure drops from P_0 to P_1 as a result of viscous friction dissipation and dynamic-static pressure conversion through the sealing device. Let the effective coverage area be S_0, and adsorption force F_a can be approximately calculated as

$$F_a = (P_0 - P_1)S_0 . \tag{8}$$

This is an isolate and isenthalpic process, during which there is an entropy increment Δs_1 of gas (free irreversible free expansion). Low-pressure air acquires a pressure rise after passing through the exergonic impeller, then it's sent to the outside of chamber (state C) as the completion of the entire thermodynamic cycle.

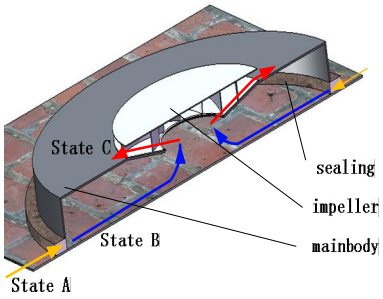

Fig. 5. Diagram of air state changes in suction circuit

In an ideal case, irreversible factors and heat transfer are neglected, BC process is seen as isentropic compression process, that is, process BC' in Fig. 6. Setting w'_s as the isentropic work on unit mass of fluid done by the fan impeller, according to thermodynamics theory:

$$w_s' = h_2 - h_1 = \frac{k}{k-1} RT_B[(\frac{P_0}{P_1})^{\frac{k-1}{k}} - 1], \tag{9}$$

where k is air's adiabatic index, R the gas constant, T_B the static temperature at the inlet of impeller. Let Q be air's mass flow rate, then the fan's shaft power W'_s is

$$W_s' = Qw_s' . \tag{10}$$

There is inevitable loss of a variety of mechanical energy in actual flow field in the impeller, characterized by the entropy rise Δs_2, BC' process is reduced to BC, a lot of work serves to compensate for energy loss. Efficiency η_{im} is introduced to calculate actual impeller shaft power as follows:

$$W_s = W_s' / \eta_{im} . \tag{11}$$

By the above simultaneous equations, it can be listed that

$$W_s = \frac{k}{k-1} RT_B[(\frac{P_0}{P_1})^{\frac{k-1}{k}} - 1] \cdot \frac{Q}{\eta_{im}} . \tag{12}$$

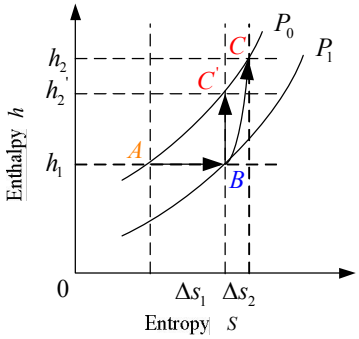

Fig. 6. Enthalpy-entropy chart

Analyse Eq. (12), since AB process is an isenthalpic process, T_B can be considered as stagnation temperature of atmosphere, which is constant and not relevant to the pressure in chamber. Therefore, when robot's size and adsorption force index are fixed, the value of W_s is only determined by Q/η_{im}. So far, the design direction is made clear, that is, to reduce flow rate and improve the efficiency of impeller. Sealing device and the vacuum level in chamber directly determine the flow rate, so that the flow resistance of seal must be enhanced to lower the flow rate when suction vacuum (finally boiling down to the index of F_a) is constant. In addition, in accordance with section 2.2, for purpose of maintaining the utilization rate of adsorption force, the increase in flow resistance should not be over-dependent on seal's positive pressure.

Improving impeller's efficiency means avoiding or restraining the energy losses such as local losses, traveling losses, boundary layer separation and frictional secondary flow, on the premise that the impeller's capacity of doing work is not affected, which requires a specific design methodology suitable for SWCR robot.

3.2 Hydromechanical analysis

Hydromechanical analysis is committed to providing technical solutions, which deduces the relationship between F_a and impeller's work through a detailed analysis of air flow's state changes in suction cycle.

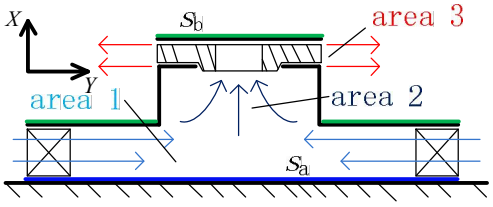

Fig. 7. Scheme of hydromechanical process

In Fig. 7, consider that the robot keeps still on the wall and neglect airflow velocity's X-component, the momentum equation in X-direction for the combination of robot's body and airflow in the chamber is expressed as

$$F_a + \iint_{s_a} (P_0 - P_{sn}(\theta, r))\mathrm{d}\sigma - \iint_{s_b} P_0 \cdot \mathrm{d}\sigma = 0, \quad (13)$$

where s_a is wall surface that is covered by robot's chamber, s_b is robot surface. P_0 is atmospheric pressure, constant. P_{sn} is negative pressure in the chamber, variable. θ, r, σ are integration variables. Eq. (13) can be reduced to

$$F_a = \iint_{s_a} P_{sn}(\theta, r)\mathrm{d}\sigma. \quad (14)$$

From Eq. (14), it is found that adsorption force only relates to the negative pressure on wall surface that is covered by robot's chamber.

High-speed airflow is concentrated close to the wall surface in the chamber, and converges in the center, then bends 90º upward to the inlet of the impeller. The rest part of the chamber is backflow zone with a little effect on adsorption characteristics. The chamber is divided into three main regions according to air's flowing characteristics, area 1, area 2, area 3 as shown in Fig. 7. Area 1 is the zone close to the wall where the high-speed air flow is concentrated, represented by dynamic and static pressure ($\rho v_1^2/2$, P_{s1}), area 2 is the zone near the impeller entrance, represented by ($\rho v_2^2/2$, P_{s2}), area 3 is the zone near the impeller outlet , represented by ($\rho v_3^2/2$, P_{s3}).

The air flows into area 1 via the sealing device from the atmospheric environment of the stagnation state. Neglecting the mechanical energy loss before entering the seal, the equation below can be listed according to energy conservation as follows:

$$P_0 = P_{m1} + \rho v_1^2/2 + P_{s1}, \quad (15)$$

where P_{m1} is energy loss after passing the seal. The effective negative pressure is

$$P_{sn} = P_0 - P_{s1} = P_{m1} + \rho v_1^2/2. \quad (16)$$

Eq. (16) shows that the effective negative pressure is composed of two parts, one is from the depressurization in the seal, and the other is converted from dynamic pressure.

According to energy conservation, the total pressure P_2 at the entrance of the impeller can be given as

$$P_2 = P_0 - P_{m1} - P_{m2} = \rho v_2^2/2 + P_{s2}, \quad (17)$$

where P_{m1} is the energy loss inside the chamber.

Air state changes from ($\rho v_2^2/2$, P_{s2}) to ($\rho v_3^2/2$, P_{s3}) after passing through the impeller, the relationship is as the following.

$$\rho v_3^2/2 = \rho v_2^2/2 + H_d, \quad (18)$$

$$P_{s3} = P_{s2} + H_s, \quad (19)$$

$$H = H_d + H_s, \quad (20)$$

where H_d, H_s, H are respectively dynamic pressure, static pressure and total pressure rise of the impeller. The air pressure recovers to atmospheric pressure from ($\rho v_3^2/2$, P_{s3}) after an energy loss at the export of impeller:

$$P_0 = \rho v_3^2/2 + P_{s3} - P_{m3}. \quad (21)$$

From Eq. (15)–(21), it can be deduced:

$$P_{sn} = H_s + \frac{1}{2}\rho v_3^2 + \frac{1}{2}\rho v_1^2 - \frac{1}{2}\rho v_2^2 - P_{m2} - P_{m3}. \quad (22)$$

The energy loss at the export of impeller P_{m3} is approximately linear to the dynamic pressure, so

$$P_{m3} = \frac{1}{2}\xi_3 \rho v_3^2, \quad (23)$$

where ξ_3 is loss constant.

Put Eq. (23) into (22) and replace the dynamic pressure with P_{d3}:

$$P_{sn} = H_s + (1-\xi_3)P_{d3} + (\frac{1}{2}\rho v_1^2 - \frac{1}{2}\rho v_2^2 - P_{m2}). \quad (24)$$

If v_2 (velocity at inlet of impeller) is made slightly less than v_1 (velocity at area 1), and P_{m2} not considerable, namely

$$\frac{1}{2}\rho v_1^2 - \frac{1}{2}\rho v_2^2 - P_{m2} = 0, \quad (25)$$

then Eq. (24) can be rewritten as

$$P_{sn} = H_s + (1-\xi_3)P_{d3}. \quad (26)$$

Eq. (26) is important for impeller design, relating impeller's aerodynamic performance to F_a. Its physical meaning is that effective negative pressure consists of two parts, one is static pressure rise of impeller, and the other is the part of dynamic pressure at the export which is effectively used.

4 Design of Impeller Specific for SWCR

4.1 Main points of design

Design method for SWCR-specific centrifugal impeller is on the basis of that for common centrifugal fans, while the unique characteristics of this method are as follows:

(1) 7-parameter method is presented, in which the parameters are inlet width B_1, outlet width B_2, inlet diameter D_1, outlet diameter D_2, inlet installation angle β_{1A},

outlet installation angle β_{2A}, blade number Z, and determine the geometry of impeller, see Fig. 8.

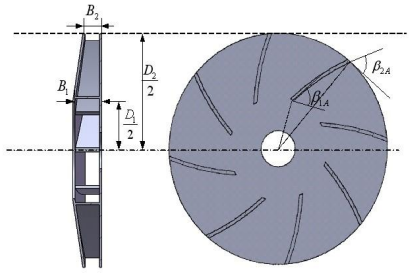

Fig. 8. 7-parameter geometric modeling of impeller

(2) Instead of goals of preconcerted flow rate and pressure ratio, the method aims at meeting the need of chamber vacuum that produces an appropriate adsorption force for SWCR to adhere and maneuver. Based on Eq. (26), the method properly allocates impeller static pressure and uses outlet kinetic energy, and ultimately attains a high-efficiency impeller that creates adequate negative pressure in the sucker.

Static pressure rise plays a major role in formation of F_a, so that the impeller with a higher static pressure ratio could obtain the same vacuum at the cost of lower power. In addition, high-static-pressure-ratio impeller has poor ability of doing work, which means that impeller needs a higher speed for the same power capability, but, high rotating speed may lead to excessive relative velocity inside the impeller, which lowers the efficiency. Therefore static pressure ratio should be selected by contrast. Moreover, when static pressure ratio is constant, with β_{2A} increasing, the adaptability to flow rate change is enhanced, which means vacuum level can be approximately maintained when there is a sudden increase in flow rate, however, corresponding B_2 gets smaller, and the internal flow velocity higher, which also brings energy loss, so β_{2A} should also be selected after comparison.

4.2 Example

In accordance with the requirements of miniaturization, specify D_2 as 100 mm, chamber vacuum 2 kPa, volume flow rate Q 0.01 m^3/s. Table 1 are obtained by calculation with the method introduced in section 4.1.

Table 1. Impeller data (Static pressure ratio Ω =0.55, 0.65)

Outlet installation angle β_{2A}/(°)	Inlet absolute velocity v_1/(m·s^{-1})		Outlet absolute velocity v_2/(m·s^{-1})		Outlet relative velocity w_2/(m·s^{-1})		Outlet width B_2/mm	
	Ω =0.55	Ω =0.65	Ω =0.55	Ω =0.65	Ω =0.55	Ω =0.65	Ω =0.55	Ω =0.65
20	2.1	6.8	51.2	43.6	6.0	19.7	16.2	5.00
30	3.3	10.7	51.2	44.4	6.6	21.4	10.2	3.10
40	4.8	15.6	51.3	45.8	7.4	24.2	7.0	2.20
50	6.8	22.2	51.6	48.5	8.9	28.9	4.9	1.50
60	9.9	32.3	52.1	53.8	11.4	37.2	3.4	1.00
70	15.8	51.4	53.5	67.0	16.8	54.6	2.1	0.65
80	32.9	107.3	60.8	115.6	33.4	108.8	1.0	0.31

From the calculation, if β_{2A} is small, relative velocity in impeller could keep at a low level, and B_2 keeps fairly large, e.g. with static pressure ratio of 0.55, when β_{2A} is 20°, w_2 is only 6 m/s and corresponding B_2 16.2 mm, at this time, its internal loss can be reduced to a negligible level. However, β_{2A} of 20° is too low to have good flow rate adaptability, the adsorption system is likely to fail with a suddenly increased flow.

When β_{2A} is constant, though increasing the static pressure ratio is helpful for converting energy to chamber vacuum more effectively, it will also cause w_2 to shoot up, e.g. with β_{2A} of 80°, w_2 reaches 108.8 m/s at the static pressure ratio of 0.65, where B_2 is only 0.31 mm, such geometric modeling is of no practical use.

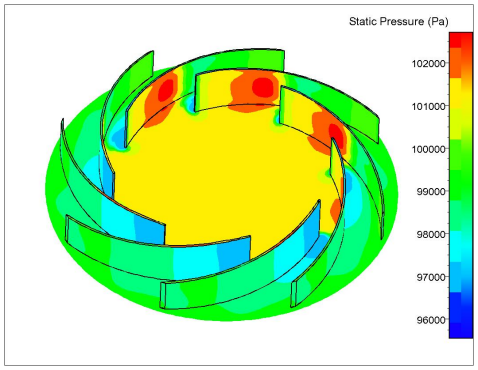

(a) β_{2A} = 20°, static pressure ratio 0.65

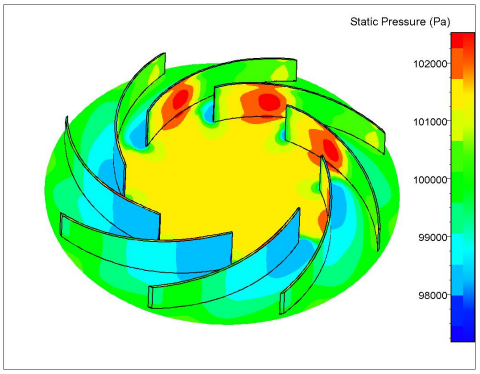

(b) β_{2A} = 25°, static pressure ratio 0.65

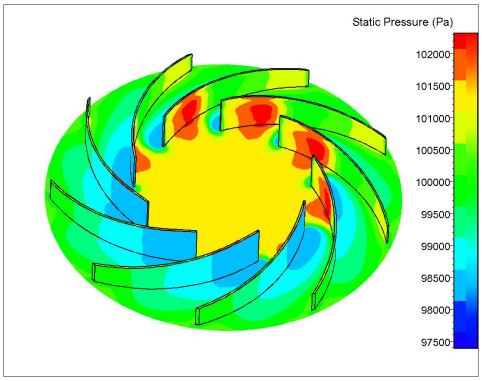

(c) β_{2A} = 30°, static pressure ratio 0.65

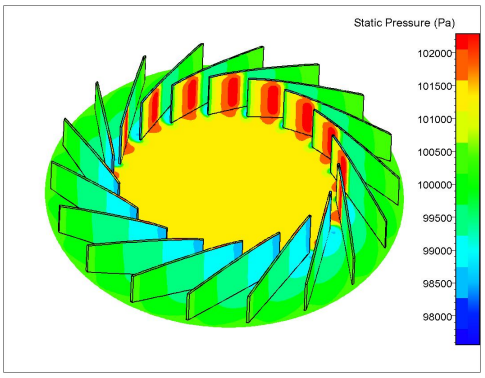

(d) β_{2A} = 50°, static pressure ratio 0.55

Fig. 9. CFD simulation of 4 impellers

Four types of impeller's aerodynamic performances at flow rate of 0.02 m^3/s are simulated by using NUMECA. They are respectively (a) β_{2A} = 20°, static pressure ratio 0.65, (b) β_{2A} = 25°, static pressure ratio 0.65, (c) β_{2A} = 30°, static pressure ratio 0.65, and (d) β_{2A} = 50°, static pressure ratio 0.55.

Now we analyse 4 impellers' simulation results, at design load of 0.02 m^3/s, *b*, *c* impeller's pressure rise is coincidence well with the design value, but, as for impeller *a*, ratio D_1/D_2 is too big, and this will make no guarantee that air flows into the impeller vertically, resulting in drop of impeller total pressure, as shown in Fig. 10, impeller *a* pressure rise is about 10% lower than that of *b*, *c*. Except a big ratio of D_1/D_2, impeller *d* has large-radius blades because its β_{2A} is rather big, affecting the flow efficiency and resulting in a further reduce in pressure rise—its pressure rise is only about 70% of that of *b* and *c*, which may cause adhesion failure. Because the 4 impellers above are all backward impellers (β_{2A}<90°), their pressure ratios all show a decreasing trend when flow rate increases.

Refer to Fig. 11, in the design conditions, *b*, *c* impeller's isentropic efficiencies have all reached a high level of nearly 90%. However, when flow rate increases, there is a visible decline in efficiency. The impellers of *a* and *d* have a long distance in both pressure ratio and efficiency compared with *b* and *c*, so the former should be the first choice for application.

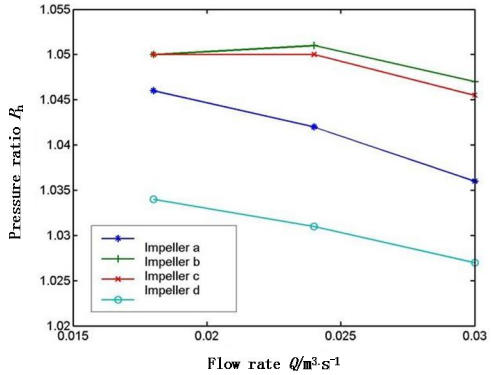

Fig. 10. Pressure ratio-flow rate chart

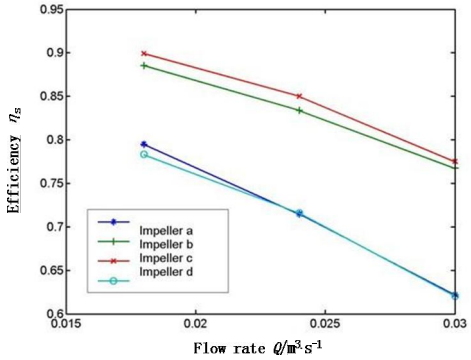

Fig. 11. Efficiency-flow rate chart

5 BIT Climber and Experimental Tests

An SWCR prototype called "BIT Climber" was developed for test, its mechanical structure is shown in Fig.12.

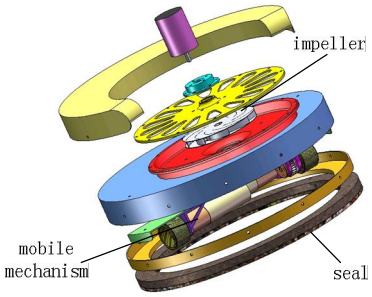

Fig. 12. Exploded view of BIT Climber

Considering the tradeoff of adsorption performance and controlling difficulty, *b* type, namely 2 driven wheels and 2 passive wheels as described in section 2.1, is used as locomotion mechanism. The robot uses a flexible rubber mat combined with a hair ring as sealing device. The rubber has big flow resistance, and its appropriate flexibility helps the robot to accommodate small obstacles in motion. The hair ring is an ascendant throttling device, it has powerful function of decompression and makes the robot adapt to relative movement against the wall.

For the purpose of designing a suitable impeller, the fluid environment where the robot works should be specified, after evaluation we set effective negative pressure to be 3 kPa, flow rate 0.02 m^3/s. The method presented in section 4 is followed for impeller primary selection, simulation and analysis. Finally, an impeller, with D_2 = 95 mm, D_1 = 42 mm, B_2 = 9.2 mm, B_1 = 15 mm, β_{2A} = 30°, β_{1A} = 15°, Z = 9, is manufactured and mounted in the robot.

Experiments were conducted to evaluate the performance of Bit Climber. The specifications are listed in Table 2. It was demonstrated that BIT Climber is able to move on various wall surfaces to perform its task, the working surfaces include brick, glass, metal, stucco, wood and

plaster, see Fig. 13.

Table 2. Specifications of BIT Climber

Mass W/kg	Height H/cm	Diameter D/cm	Payload capacity P_c/kg	Step clearance S_c/cm	Velocity V/(m•s^{-1})
2.6	5.0	30	5	0.5	0–5

Fig. 13. BIT Climber at work with a load of 59 N

The adsorption force F_a is 208 N, of which 9 N is F_{ss}, 30 N is F_{sp}, the utilization rate of adsorption force is 81%. Average vacuum in the sucker is 2.94 kPa, electric power of impeller shaft is about 150 W, reaching a relatively high utilization rate of power of about 84%.

6 Conclusions

(1) The paper illustrates how mobile mechanism and pressure allocation for sealing device influence SWCR's utilization rate of adsorption force, providing a theoretical basis for relevant parameters selection.

(2) Suction system's thermodynamics and hydrodynamics analysis is presented, which shows that reducing flow rate and improving the efficiency of impeller are directions for improving utilization rate of power.

(3) The paper comes up with a design method for SWCR-specific impeller, in which outlet installation angle and static pressure ratio are two key parameters that impact its aerodynamic performance.

(4) Through development of prototype and experiments, conclusions above are verified. Future work focuses on the premise of good maneuverability and adsorption performance, how to reduce flow rate to save power remarkably.

References

[1] MASATAKA S, SHINYA K, SHIGEO H. Basic systematic experiments and new type child unit of anchor climber: awarm type wall climbing robot system[C]//*Proceedings of IEEE Int. Conf. on Robotics and Automation*, Pasadena, USA, May 19-23, 2008: 3 034–3 039.

[2] SHANG Jianzhong, BRIDGE B, SATTAR T, et al. Development of a climbing robot for inspection of long weld lines[J]. *Industrial Robot: An International Journal*, 2008, 35(3): 217–223.

[3] KALRA L P, GU J. An autonomous self contained wall climbing robot for non-destructive inspection of above-ground storage tanks [J]. *Industrial Robot: An International Journal*, 2007, 34(2):122–127.

[4] XU Zeliang, MA Peisun. A wall-climbing robot for labelling scale of oil tank's volume[J]. *Robotica*, 2002, 20(2):209–212.

[5] KIM S, SPENKO M, TRUJILLO S, et al. Smooth vertical surface climbing with directional adhesion[J]. *IEEE Transactions on Robotics*, 2008, 24(1): 65–74.

[6] ASBECK A T, KIM S, CUTKOSKY M R, et al. Scaling hard vertical surfaces with compliant microspine arrays[J]. *International Journal of Robotics Research*, 2006, 25(12): 1 165–1 179.

[7] ZHAO Boxin, PESIKA N, ROSENBERG K, et al. Adhesion and friction force coupling of gecko setal arrays: Implications for structured adhesive surfaces[J]. *Langmuir*, 2008, 24(4): 1 517–1 524.

[8] MICHAEL P M, WILLIAM T, MICHAEL T, et al. Waalbot: an agile small-scale wall climbing robot utilizing pressure sensitive adhesives[C]//*Proceedings of IEEE Int. Conf. on Intelligent Robots and Systems*, Beijing, China, October 9-15, 2006: 3 411–3 416.

[9] AKIHIKO N, SHIGEO H. Walking and running of the quadruped wall-climbing robot[C]//*Proceedings of IEEE International Conference on Robotics and Automation*, San Diego, USA, May 8-13, 1994: 1 005–1 012.

[10] BACH F W, RACHKOV M, SEEVERS J, et al. High tractive power wall-climbing robot[J]. *Automation in Construction*, 1995, 4(3): 213–224.

[11] YANO T, SUWA T, MURAKAMI M, et al. Development of a semi self-contained wall climbing robot with scanning type suction cups[C]//*Proceedings of IEEE International Conference on Intelligent Robots and Systems*, Grenoble, France, Sept. 7-11, 1997: 900–905.

[12] KEISUKE A, SHIGEO H. Study of walking robot for 3 dimensional terrain[C]//*Proceedings of IEEE International Conference on Robotics and Automation*, Nagoya, Japan, May 21-27, 1995: 703–708.

[13] GUIDO L R, MICHELE M, GIOVANNI M, et al. A low-cost lightweight climbing robot for the inspection of vertical surface[J]. *Mechatronics*, 2002, 12(1): 71–96.

[14] LAL T R, MUKHERJEE R, NING Xi, et al. Climbing the walls[J]. *IEEE Robotics & Automation Magazine*, 2002, 9(4): 10–19.

[15] SUN Dong, ZHU Jian, LAI Chiming, et al. A visual sensing application to a climbing cleaning robot on the glass surface[J]. *Mechatronics*, 2004, 14(10): 1 089–1 104.

[16] ZHANG Houxiang, ZHANG Jianwei, ZONG Guanghua, et al. Sky Cleaner 3: a real pneumatic climbing robot for glass-wall cleaning[J]. *IEEE Robotics & Automation Magazine*, 2006, 13(1): 32–41.

[17] JUN Xiao, XIAO Jizhong, NING Xi, et al. Fuzzy controller for wall-climbing microrobots[J]. *IEEE Transactions on Fuzzy Systems*, 2004, 12(4): 466–480.

[18] QIAN Zhiyuan, ZHAO Yanzheng, FU Zhuang, et al. Design and realization of a non-actuated glass-curtain wall-cleaning robot prototype with dual suction cups[J]. *International Journal of Advanced Manufacturing Technology*, 2006, 30(1): 147–155.

[19] MATTHEW E, WILLIAM M, ANGEL C, et al. City-Climbers at work[C]//*Proceedings of IEEE International Conference on Robotics and Automation*, Roma, Italy, April 10-14, 2007: 2 764–2 765.

[20] XIAO Jizhong, SADEGH A, MATTHEW E, et al. Design of mobile robots with wall climbing capability[C]//*Proceedings of IEEE/ASME International Conference on Advanced Intelligent Mechatronics*, Callfornla, USA, July 24-28, 2005: 438–443.
[21] WU Shanqiang, CHEN Xiaodong, LI Mantian, et al. Dynamic pressure analysis and experimental research of a wall-climbing robot[J]. *Optics and Precision Engineering*, 2008, 16(3): 478–483. (in Chinese)
[22] HILLENBRAND C, SCHMIDT D, BERNS K. CROMSCI: development of a climbing robot with negative pressure adhesion for inspections[J]. *Industrial Robot*: *An International Journal*, 2008, 35(3): 228–237.
[23] LONGO D, MUSCATO G. The Alicia 3 Climbing Robot[J]. *IEEE Robotics & Automation Magazine*, 2006, 13(1): 42–50.
[24] DOMENICO L, GIOVANNI M. A modular approach for the design of the Alicia3 climbing robot for industrial inspection[J]. *Industrial Robot: An International Journal*, 2004, 31(2): 148–158.
[25] QIN Shanxing, LIU Rong, XU Zhenxiang, Optimization design of pressure distribution for mini wall-climbing robot[J]. *Dual Use Technologies & Products*, 2007, 2(1): 47–48. (in Chinese)

Biographical notes

LI Jun, born in 1983, is currently a PhD candidate in School of Mechatronical Engineering, Beijing Institute of Technology, China. He received his bachelor degree from Beijing Institute of Technology, China, in 2005. His research interest is wall-climbing robots.
E-mail: luvelva@bit.edu.cn.

GAO Xueshan, born in 1966, is currently an associate professor and a PhD candidate supervisor in School of Mechatronical Engineering, Beijing Institute of Technology, China. His interests include mobile robot, medical robot, evolutionary robot and new robotic mechanism. He is a senior member of Chinese Mechanical Engineering Society (CMES) and a member of IEEE.
E-mail: xueshan.gao@bit.edu.cn

FAN Ningjun, born in 1949, is currently a professor in School of Mechatronical Engineering, Beijing Institute of Technology, China. His research interests include integration technology of miniature system, mechatronics and special robots.
E-mail: fanningj@publicb.bta.net.cn

LI Kejie, born in 1946, is currently a professor in School of Mechatronical Engineering, Beijing Institute of Technology, China. His research interests are wireless sensor network, design and integration of miniature system, robot sensor and sensing system.
E-mail: likj@bit.edu.cn

JIANG Zhihong, born in 1974, is currently an associate professor in School of Mechatronical Engineering, Beijing Institute of Technology, China. His research interests include power electronics, motor driver and robot control.
E-mail: jiangzhihong@bit.edu.cn

JIANG Zhijian, born in 1964, is currently a professor in School of Electric and Information Engineering, Beijing University of Civil Engineering and Architecture, China. His research interests include electronics and architectural robots.
E-mail: jzjmail@bucea.edu.cn